Accepted Manuscript

A-site ordered state in manganites with perovskite-like structure based on the optimally doped compounds Ln0.70Ba0.30MnO3 (Ln = Pr, Nd)

S.V. Trukhanov, V.A. Khomchenko, D.V. Karpinsky, M.V. Silibin, A.V. Trukhanov, L.S. Lobanovsky, H. Szymczak, C.E. Botez, I.O. Troyanchuk

PII: S1002-0721(18)30785-3

DOI: https://doi.org/10.1016/j.jre.2018.12.010

Reference: JRE 380

To appear in: *Journal of Rare Earths*

Received Date: 24 September 2018

Revised Date: 7 December 2018

Accepted Date: 10 December 2018

Please cite this article as: Trukhanov SV, Khomchenko VA, Karpinsky DV, Silibin MV, Trukhanov AV, Lobanovsky LS, Szymczak H, Botez CE, Troyanchuk IO, A-site ordered state in manganites with perovskite-like structure based on the optimally doped compounds Ln0.70Ba0.30MnO3 (Ln = Pr, Nd), *Journal of Rare Earths*, https://doi.org/10.1016/j.jre.2018.12.010.

A-site ordered state in manganites with perovskite-like structure based on the optimally doped compounds $Ln_{0.70}Ba_{0.30}MnO_3$ (Ln = Pr, Nd)

S.V. Trukhanov[1,2,3*], V.A. Khomchenko[4], D.V. Karpinsky[3,5], M.V. Silibin[3,5,6], A.V. Trukhanov[1,2,3], L.S. Lobanovsky[3], H. Szymczak[7], C. E. Botez[8], I. O. Troyanchuk[3,5]

[1] *National University of Science and Technology MISiS, 119049, Moscow, Leninsky av., 4, Russia*
[2] *South Ural State University, 454080, Chelyabinsk, Lenin av., 76, Russia*
[3] *Scientific- Practical Materials Research Centre of NASB, 220072 Minsk, Belarus*
[4] *CFisUC, Department of Physics, University of Coimbra, 3004-516 Coimbra, Portugal*
[5] *National Research University of Electronic Technology "MIET", 124498 Zelenograd, Moscow, Russia*
[6] *Institute for Bionic Technologies and Engineering, I.M. Sechenov First Moscow State Medical University, 2-4 Bolshaya Pirogovskaya st., Moscow, 119991, Russia*
[7] *Institute of Physics, Polish Academy of Sciences, 02-668, Warsaw, Poland*
[8] *The University of Texas at El Paso, El Paso, TX 79968-0515, USA*

Foundation item: Project supported by the European Union's Horizon 2020 Research and Innovation Programme under the Marie Sklodowska-Curie grant agreement No. 778070.

** corresponding author: email: sv_truhanov@mail.ru; phone: +375-17-284-11-68*

Abstract: In this paper, we report on the crystal structure and magnetic properties of the nanostructured Ba-ordered phases of rare-earth manganites obtained from the optimally doped solid solutions $Ln_{0.70}Ba_{0.30}MnO_3$ (Ln = Pr, Nd). The materials were studied by X-ray diffraction, scanning electron microscopy, energy dispersive spectroscopy and SQUID-magnetometry techniques. It is found that states with different degrees of cation ordering in the *A*- sublattice of the ABO_3 perovskite can be obtained by employing special conditions of chemical treatment. In particular, reduction of the parent compounds results in the formation of a nanocomposite containing ferrimagnetic anion-deficient ordered phase $LnBaMn_2O_5$. Oxidation of the composite does not change an average size of the nanocrystallites, but drastically alters their phase composition to stabilize ferromagnetic stoichiometric ordered phase $LnBaMn_2O_6$ and ferromagnetic superstoichiometric disordered phase $Ln_{0.90}Ba_{0.10}MnO_{3+\delta}$. It is shown that the magnetic properties of the materials are determined by the joint action of chemical (cation ordering) and external (surface tension) pressures.

Keywords: Ionic order, Magnetic transition; Perovskite; Magnanite; Rare earths

1. Introduction

The discovery of the colossal magnetoresistance effect in hole-doped manganites with the perovskite-type structure [1,2] has renewed the interest in the $Ln_{1-x}A_xMnO_3$ (Ln is a lanthanide) systems which, in fact, have been known for a long time [3- 9]. Nowadays manganites are the model objects for the physics of strongly correlated electronic systems. These materials demonstrate a variety of magnetic and structural phase transitions, charge and orbital ordering, magnetic and structural phase separation, pressure-induced insulator-to-metal transitions and many others intriguing physical phenomena [10,11]. However, despite the numerous investigations, the nature of the interplay between the lattice, orbital,

charge, and spin degrees of freedom is still a matter of discussion. Physical properties of the layered manganites $LnBaMn_2O_6$ (demonstrating the ordered cation arrangement in the A sublattice of the perovskite) are one of the most interesting topics in this field [12–21]. The main structural feature of these Ba-ordered compounds is an alternation of MnO_2 planes with LnO and BaO planes completely filled with one type of cations; as a result, the MnO_6 octahedra are periodically distorted. In contrast to solid solutions $Ln_{0.5}Ba_{0.5}MnO_3$, where the substituting cations are statistically distributed [22], the physical properties of the ordered manganites $LnBaMn_2O_6$ are significantly affected by the local periodic lattice distortions.

It has been previously shown that the Ba-ordered compounds can be obtained using topotactic redox reactions [23–25]. Oxygen-stoichiometric solid solutions $Ln_{0.5}Ba_{0.5}MnO_3$, synthesized in air using a conventional ceramic technology, have a cubic lattice (space group $Pm\,\bar{3}\,m$) with random distribution of Ln^{3+} and Ba^{2+} cations. Anion-deficient compounds $LnBaMn_2O_5$, obtained by annealing the solid solutions $Ln_{0.5}Ba_{0.5}MnO_3$ in a reducing environment, possess a tetragonal unit cell (P4/mmm) with ordered distribution of Ln^{3+} and Ba^{2+}. The basal planes of a perovskite cuboctahedron are completely filled by one type of ions and alternate along the [001] direction. Oxygen vacancies are concentrated in the planes LnO_x containing a lanthanide. Such a crystal structure is similar to the structure of $YBaCuFeO_5$ [26]. Oxidation of the anion-deficient compounds $LnBaMn_2O_5$ in air leads to the formation of the stoichiometric Ba-ordered compounds $LnBaMn_2O_6$, whose unit cell is also tetragonal (P4/mmm). Magnetic properties of the materials strongly depend on degree of the cation ordering [27, 28]. The following questions arise: can the Ba-ordered state be stabilized in solid solutions with $Ln^{3+}/Ba^{2+} \neq 1/1$? What is the mechanism of such an ordering? We investigated the so-called optimally doped solid solutions $Ln_{0.70}Ba_{0.30}MnO_3$ (Ln = Pr, Nd) to answer these questions.

2. Experimental

Polycrystalline samples of $Ln_{0.70}Ba_{0.30}MnO_3$ (Ln = Pr, Nd) were obtained using a conventional ceramic technology. Oxides Pr_6O_{11}, Nd_2O_3, Mn_2O_3 and carbonate $BaCO_3$ were weighed in accordance with the cation ratio Ln : Ba : Mn= 0.70 : 0.30 : 1.00, thoroughly mixed and pressed. Decarbonization was carried out by annealing the samples in air at T = 1100 °C for 2 h, followed by grinding. The final synthesis was performed in air at T = 1560 °C for 2 h. The equations for the chemical reaction for the optimally doped Ba-substituted praseodymium and neodymium manganites can be written in the form

$$(0.70/6)Pr_6O_{11} + 0.30BaCO_3 + 0.50Mn_2O_3 \rightarrow Pr_{0.70}Ba_{0.30}MnO_3 + 0.30CO_2 \uparrow \quad (1)$$

$$0.35Nd_2O_3 + 0.30BaCO_3 + 0.50Mn_2O_3 \rightarrow Nd_{0.70}Ba_{0.30}MnO_3 + 0.30CO_2 \uparrow \quad (2)$$

To obtain solid solutions with the oxygen content close to the stoichiometric value, the samples were cooled down to room temperature at a rate of 100 °C/h [29]. The oxygen content was determined using a thermogravimetric analysis [30], which showed that the samples had the stoichiometric oxygen concentration.

Anion-deficient compounds were obtained by the method of topotactic reactions. The samples were placed in evacuated ($P \sim 10^{-4}$ Pa) quartz ampoules together with a certain amount of metallic tantalum, which was used as an oxygen absorber. The quartz ampoules with the samples were annealed at T = 800 °C for 24 h and then cooled down to room temperature at a rate of 100 °C/h. The reduction was carried out to the nominal phase with

"$O_{2.60}$" to satisfy the condition $Mn^{3+}/Mn^{2+}\sim 1$. The equation for this chemical reaction has the form

$$Ln_{0.70}Ba_{0.30}MnO_3 + 0.16Ta \rightarrow Ln_{0.70}Ba_{0.30}MnO_{2.60} + 0.08Ta_2O_5 \quad (3)$$

Oxygen content in the anion- deficient compounds was checked by weighing the samples before and after the reaction. The results of the experiments proved that we failed to obtain the single-phase compounds $Ln^{3+}_{0.7}Ba^{2+}_{0.3}Mn^{3+}_{0.5}Mn^{2+}_{0.5}O^{2-}_{2.6}$. The actual chemical formula of the anion- deficient samples can be written in the form

$$Pr_{0.70}Ba_{0.30}MnO_{2.60} \rightarrow ¼(1.20PrBaMn_2O_5 + [1.60/6]Pr_6O_{11} + 1.60MnO) \quad (4)$$
$$Nd_{0.70}Ba_{0.30}MnO_{2.60} \rightarrow ¼(1.20NdBaMn_2O_5 + 0.80Nd_2O_3 + 1.60MnO) \quad (5)$$

The reduced samples were oxidized in air at T = 800 °C for 3 h to obtain the nominal phase "$O_{3+\delta}$". Oxygen content was also determined by weighing the samples. To optimize the magnetic properties of the oxidized samples, the latter were additionally annealed in air at T = 800 °C for 10 h. The additional annealing at a moderate temperature did not change the oxygen content, but favored the ordering of the Ln^{3+} and Ba^{2+} cations. Subsequent investigations showed that the actual chemical formula of the oxidized product was

$$Ln_{0.70}Ba_{0.30}MnO_{3+\delta} \rightarrow ¼(LnBaMn_2O_6 + 2Ln_{0.90}Ba_{0.10}MnO_{3+\delta}) \quad (6)$$

Phase analysis of the samples and investigation of their crystal structure were performed by X-ray diffraction (XRD) technique using a DRON-3M diffractometer with Cu K_α radiation. Room- temperature XRD patterns were collected over an angular range $15° \le 2\theta \le 80°$ with a step of 0.02° and an exposition interval of 15 s/step. The data were analyzed by the Rietveld method [31] using the FullProf program [32]. Elemental analysis and investigation of surface topography were carried out with a LEO1455VP (Carl-Zeiss) scanning electron microscope. Magnetic properties of the samples were investigated with a superconducting quantum interference device (SQUID) magnetometer (MPMS-7, Quantum Design). Temperature dependences of the magnetization were measured in a weak magnetic field of 100 Oe in the temperature range 3 – 350 K in zero field cooling (ZFC) and field cooling (FC) modes. The magnetic transition temperatures were determined as inflection points on the temperature dependences of the FC magnetization (correspond to $\min\{\frac{dM_{FC}}{dT}\}$). Field dependences of the magnetization were obtained at 3 and 300 K in the magnetic field ranging from –70 to 70 kOe.

3. Results and Discussion

The Rietveld refinement of the XRD patterns obtained for the parent solid solutions $Ln_{0.70}Ba_{0.30}MnO_3$ shows that the compounds possessed orthorhombic structure with space group *Imma*. These results are consistent with the data of the previous structural investigations [33–36] where *Imma* or equivalent space group *Ibmm* has been used to describe the crystal structure of the initial compounds. A good agreement between the observed and calculated XRD patterns obtained for the $Ln_{0.70}Ba_{0.30}MnO_3$ samples is shown in Fig. 1(a). XRD experiment performed for the anion-deficient compounds obtained by annealing the $Ln_{0.70}Ba_{0.30}MnO_3$ samples in vacuum revealed a complex character of the

diffraction pattern, suggesting a multiphase structural state of the samples (Fig. 1 (b)). A thorough analysis of the diffraction data allows us to conclude that the resulting XRD profile corresponds to a superposition of three structural components. The dominant contribution (~65%) is related to anion-deficient Ba-ordered phase $LnBaMn_2O_5$ with tetragonal (space group *P4/mmm*) perovskite-like unit cell. Two other components (~25% and ~10%) are attributed to Pr_6O_{11} (Nd_2O_3) (space group $P\bar{3}m1$) and MnO (space group $Fm\bar{3}m$) phases, respectively. XRD patterns collected for the samples obtained by oxidation of the reduced compounds were successfully treated using a two-phase structural model (Fig. 1(c)). The samples consist of stoichiometric Ba-ordered phase $LnBaMn_2O_6$ with tetragonal (space group *P4/mmm*) unit cell (~ 60%), and superstoichiometric Ba-disordered phase $Ln_{0.90}Ba_{0.10}MnO_{3+\delta}$ with orthorhombic (space group *Pnma*) lattice (~40%). These results are also in good agreement with the available data [25, 37–39]. Additional annealing of the oxidized samples in air does not change their structural characteristics significantly. Unit cell parameters, atomic coordinates, and interatomic distances and angles characteristic of the mentioned perovskite-type phases at room temperature are presented in Tables 1 and 2.

It should be noted that the similar solid solutions having La ions in the A-position exhibit different pattern of changes in the crystal and magnetic structures upon decrease of the oxygen content. In the $La_{0.7}Ba_{0.3}MnO_{3-\delta}$ samples, the decrease in the oxygen concentration down to δ=0.4 does not cause a modification of the cubic crystal structure specific to the oxygen-stoichiometric material [40]. Accordingly, magnetic properties of the solid solutions $La_{0.7}Ba_{0.3}MnO_{3-\delta}$ ($\delta \leq 0.4$) undergo significantly different evolution [41] as compared to that observed for the compounds $Ln_{0.7}Ba_{0.3}MnO_{3-\delta}$ (Ln= Pr, Nd) (will be described below).

Fig. 2 schematically shows crystal structure of the perovskite-like phases found in the series under study. The ideal perovskite structure has ABO_3 stoichiometry and consists of a three-dimensional framework of corner-linked BO_6 octahedra. The twelve coordinated A-cations fill the cavities formed by the framework. This arrangement of ions generates a crystal structure described by the space group $Pm\bar{3}m$. In most perovskite-type oxides, due to the small radius of the *A*-site ion with respect to its surrounding cage, the BO_6 octahedra tilt to accommodate the *A* ion. For $Ln_{0.70}Ba_{0.30}MnO_3$, the rotation along the [110] direction yields the orthorhombic space group *Imma* (Fig. 2(a)). For the anion-deficient Ba-ordered phase $LnBaMn_2O_5$, cations Ln^{3+} and Ba^{2+} are located in the planes alternating along the [001] direction. Oxygen vacancies lie in the LnO_x planes containing Ln^{3+} cations. The Mn^{3+} and Mn^{2+} ions lie in oxygen pentahedra. As a result of the ordering of the cations and oxygen vacancies, the unit cell is doubled to give the tetragonal symmetry *P4/mmm* (Fig. 2 (b)). For the stoichiometric Ba-ordered phase $LnBaMn_2O_6$, the structural pattern is similar to that of the anion-deficient phase, but all the oxygen vacancies are occupied. The Mn^{3+} and Mn^{4+} cations are distributed statistically among oxygen octahedra (Fig. 2 (c)). The superstoichiometric Ba-disordered phase $Ln_{0.90}Ba_{0.10}MnO_{3+\delta}$ has an ionic arrangement typical of the parent compounds $LnMnO_3$ [42] (Fig. 2 (d)).

Scanning electron microscopy found a remarkable change in the crystallite size of the samples after the redox reaction (Fig. 3). The noticeable decrease in the average crystallite size for the oxidized Ba-ordered nanocomposite ¼($LnBaMn_2O_6$ + 2$Ln_{0.90}Ba_{0.10}MnO_{3+\delta}$) from $\langle D \rangle$ ~ 5 μm to $\langle D \rangle$ ~ 100 nm can be explained by an intensive ionic diffusion as well as by the ordering of oxygen vacancies in the form of the complex surfaces over which the destruction of the material takes place [43]. To a certain extent, the size of the crystallites can determine structural properties of the material.

Indeed, comparison of the unit cell volumes characteristic of crystal structure of the stabilized phases with those reported in literature [34, 38] suggests that the decrease in the grain size to a nanometer scale reduces the unit cell volume; the effect can be explained by an increase of the surface tension in the surface layer of nanocrystallites as compared to the microcrystallite bulk materials [44].

Magnetic properties of the materials are summarized in Figs. 4–8. In accordance with the rules for the superexchange interaction Mn^{3+}–O–Mn^{4+} [8, 9], the parent Ba-disordered solid solution $Pr_{0.70}Ba_{0.30}MnO_3$ demonstrates a ferromagnetic behavior below the Curie temperature $T_C \approx 173$ K (Fig. 4(a), Fig. 7). The anion-deficient Ba-ordered nanocomposite ¼(1.20$PrBaMn_2O_5$ + [1.60/6]Pr_6O_{11} + 1.60MnO), whose main perovskite-like phase contains manganese ions with the average valency $Mn^{2.5+}$, possesses the properties characteristic of ferrimagnets ($T_N \approx 113$ K) (Fig. 4(b), Fig. 7). The FC dependence of the magnetization obtained for the oxidized Ba-ordered nanocomposite ¼($PrBaMn_2O_6$ + 2$Pr_{0.90}Ba_{0.10}MnO_{3+\delta}$) exhibits two anomalies at ~ 313 and ~ 138 K, which correspond to the transitions from ferromagnetic to paramagnetic state for the $PrBaMn_2O_6$ and $Pr_{0.90}Ba_{0.10}MnO_{3+\delta}$ phases, respectively (Fig. 4(c), Fig. 7). A very similar behavior was found for the Nd-containing samples (Fig. 5, Fig. 8). Additional annealing of the nanocomposites ¼($LnBaMn_2O_6$ + 2$Ln_{0.90}Ba_{0.10}MnO_{3+\delta}$) in air gives rise to more sharp magnetic transitions. The Curie temperatures remain the same (Fig. 6).

Significant increase in the magnetic transition temperatures observed for the stoichiometric Ba-ordered phases can be explained by increasing the average angle ⟨Mn–O–Mn⟩ (Tables 1 and 2). Indeed, it is well known that such increasing enhances intensity of the superexchange interactions Mn–O–Mn. An analogous high sensitivity of the Curie temperature to a change in the average bond angle was observed in some previous works [45,46]. Slight decrease of the magnetization observed for the oxidized Pr-based samples (Fig. 7(a)) can be explained by the existence of antiferromagnetic clusters with charge/orbital ordering [19,31,47,48]. The superstoichiometric Ba-disordered phases $Ln_{0.90}Ba_{0.10}MnO_{3+\delta}$ exhibit higher Curie temperatures as compared to $T_C \approx 110$ K (Ln = Pr) and $T_C \approx 97$ K (Ln = Nd) reported for microcrystallite bulk materials [37, 38]. This can be attributed to the effect of nanocrystallite compression and the presence of superstoichiometric Mn^{4+} cations.

4. Conclusions

Structure and magnetic properties of the Ba-ordered phases obtained via a chemical treatment of $Ln_{0.70}Ba_{0.30}MnO_3$ (Ln = Pr, Nd) manganites were investigated. The parent Ba-disordered solid solutions $Ln_{0.70}Ba_{0.30}MnO_3$ were synthesized in air according to a conventional ceramic technology. The compounds are characterized by orthorhombic *Imma* structure and are ferromagnetic with $T_C \approx 173$ K and $T_C \approx 143$ K for Ln = Pr and Ln = Nd, respectively. The average size $\langle D \rangle$ of crystallites in the samples is about 5 μm. Reduction of the parent samples results in their separation into three phases: the anion-deficient ordered phase $LnBaMn_2O_5$ having tetragonal *P*4/*mmm* structure, and the simple-oxide phases Ln_2O_3 and MnO. The reduction leads to the formation of the nanocomposite with the average crystallite size $\langle D \rangle$~100 nm. The anion-deficient Ba-ordered phase $LnBaMn_2O_5$ exhibits ferrimagnetic properties with $T_N \approx 113$ K and $T_N \approx 123$ K for Ln = Pr and Ln = Nd, respectively. Oxidation of the anion- deficient samples does not change the average size of the nanocrystallites, but noticeably alters their phase composition. The oxidized nanocomposites consist of two perovskite-like phases. The stoichiometric Ba-ordered phase $LnBaMn_2O_6$ has tetragonal *P*4/*mmm* structure and is ferromagnetic with $T_C \approx$ 313 K (Ln = Pr) and $T_C \approx 303$ K (Ln = Nd). The superstoichiometric Ba-disordered phase

$Ln_{0.90}Ba_{0.10}MnO_{3+\delta}$ possesses orthorhombic *Pnma* lattice and has $T_C \approx 138$ K (Ln = Pr) and $T_C \approx 123$ K (Ln = Nd). Magnetic properties of the compounds under study are discussed taking into account the effect of the joint action of the chemical (cation ordering) and external (surface tension) pressures.

Acknowledgements: V.A.K. acknowledge FCT (projects UID/FIS/04564/2016 and IF/00819/2014/CP1223/CT0011), M.V.S. and D.V.K. acknowledge RFBR (#17-58-45026 IND_a) and MK-1720.2017.8. S.V. T and A.V. T acknowledge financial support from the Ministry of Education and Science of the Russian Federation in the framework of Increase Competitiveness Program of NUST «MISiS» (grants No. П02-2017-2-4 and No. К3-2018-026) and SUSU (Government task in SUSU 5.5523.2017/8.9).

References:

1. Helmolt R, Wecker J, Holzapfel B,Schultz L, Samwer K. Giant negative magnetoresistance inperovskitelike $La_{2/3}Ba_{1/3}MnO_x$ ferromagnetic films. *Phys Rev Lett.* 1993;71:2331.

2.TroyanchukIO, TrukhanovSV, KhalyavinDD, SzymczakH.Magnetic properties of anion deficit manganites $Ln_{0.55}Ba_{0.45}MnO_{3-\gamma}$ (Ln=La, Nd, Sm, Gd, $\gamma \leq 0.37$). *J Magn Magn Mater*.2000;208:217.

3. Wollan EO, Koehler WC. Neutron diffraction study of the magnetic properties ofthe series of perovskite-type compounds $[(1-x)La,xCa]MnO_3$. *Phys Rev*.1955;100:545.

4. Zener C. Interaction between the d-Shells in the transition metals. II. Ferromagneticcompounds of manganese with perovskite structure. *Phys Rev.* 1951;82:403.

5. De Gennes PG. Effects of double exchange in magnetic crystals. *Phys. Rev*.1960;118:141.

6. Goodenough JB, Wold A, Arnot RJ, Menyuk N. Relationship between crystalsymmetry and magnetic properties of ionic compounds containing Mn^{3+}. *Phys Rev.*1961;124:373.

7. Trukhanov SV, Kasper NV, Troyanchuk IO, Tovar M, Szymczak H, Bärner K. Evolution of Magnetic State in the $La_{1-x}Ca_xMnO_{3-\gamma}$ (x = 0.30, 0.50) manganites depending on the oxygen content. *J Sol State Chem.* 2002:169;85.

8. Trukhanov SV, Lobanovski LS, Bushinsky MV, Khomchenko VA, Pushkarev NV, Tyoyanchuk IO, et al. Influence of oxygen vacancies on the magnetic and electrical properties of $La_{1-x}Sr_xMnO_{3-x/2}$ manganites. *Eur Phys J B.* 2004;42:51.

9. Trukhanov SV. Investigation of stability of ordered manganites. *JETP* 2005;101:513.

10. Dagotto E, Hotta T, Moreo A. Colossal magnetoresistant materials: the key role of phase separation. *Phys Reports.* 2001;344:1.

11. Dagotto E, Tokura Y. Strongly correlated electronic materials: present and future. *MRS Bull.* 2008;33:1037.

12. Nakajima T, Kageyama H, Ichihara M, OhoyamaK, YoshizawaH, UedaY. Anomalous octahedral distortion andmultiple phase transitions in the metal-ordered manganite $YBaMn_2O_6$. *J Solid State Chem.* 2004;177:987.

13. Ueda Y, Nakajima T. Novel structures and electromagnetic properties of the A-siteordered/disordered manganites $RBaMn_2O_6/R_{0.5}Ba_{0.5}MnO_3$ (R = Y and rare earthelements). *J Phys Condens Matter.* 2004;16:S573.

14. Vidya R, Ravindran P, Vajeeston P,KjekshusA, FjellvågH. Effect of oxygen stoichiometry on spin, charge, and orbital ordering in manganites. *Phys Rev B.* 2004;69:092405.

15. Karppinen M, Okamoto H, Fjellvåg H, Motohashi T, Yamauchi H. Oxygen and cation ordered perovskite, $Ba_2Y_2Mn_4O_{11}$. *J Solid State Chem.* 2004;177:2122.

16. Takeshita N, Terakura C, Akahoshi D, Tokura Y, Takagi H. Pressure-induced transition from a spinglass to an itinerant ferromagnet in the half-doped manganite $L_{0.5}Ba_{0.5}MnO_3$ (L=Sm andNd) with quenched disorder. *Phys Rev B.* 2004;69:180405(R).
17. Nakajima T, Ueda Y. Structures and electromagnetic properties of the A-sitedisordered Ba-based manganites; $R_{0.5}Ba_{0.5}MnO_3$ (R = Y and rare earth elements) *J Alloys Compd.* 2004;383:135.
18. Nakajima T, Kageyama H, Ueda Y. Dramatic change of magnetic property in theA-site ordered/disordered manganites $PrBaMn_2O_6$/$Pr_{0.5}Ba_{0.5}MnO_3$. *J Magn Magn Mater.* 2004;272-276:405.
19. Nakajima T, Yoshizawa H, Ueda Y. A-site randomness effect on structural andphysical properties of Ba-based perovskite manganites. *J Phys Soc Jpn.*2004:73:2283.
20. Sfirloaga P, Poienar M, Malaescu I, Lungu A, Vlazan P. Perovskite type lanthanum manganite: Morpho-structural analysis and electrical investigations. *J Rare Earths.* 2018;36:499.
21. Thaljaoui R, Pękała M, Fagnard JF, Vanderbemden Ph. Effect of Ag substitution on structural, magnetic and magnetocaloric properties of $Pr_{0.6}Sr_{0.4-x}Ag_xMnO_3$ manganites. *J Rare Earths.* 2017;35:875.
22. Akahoshi D, Uchida M, Tomioka Y, ArimaT, MatsuiY, TokuraY. Random potential effect near the bicriticalregion in perovskite manganites as revealed by comparison with the ordered perovskite analogs. *Phys Rev Lett.* 2003;90:177203.
23. Millange F, Caignaert V, Domenges B, Raveau B. Order-disorder phenomena in new $LaBaMn_2O_{6-x}$ CMR perovskites. Crystal and magnetic structure. *Chem Mater.*1998;10:1974.
24. Troyanchuk IO, Trukhanov SV, Szymczak H, Baerner K. Effect of oxygen contenton the magnetic and transport properties of $Pr_{0.5}Ba_{0.5}MnO_{3-\gamma}$. *J Phys Condens Matter.* 2000;12:L155.
25. Trukhanov SV, Troyanchuk IO, Hervieu M, Szymczak H, Bärner K. Magnetic and electrical properties of $LBaMn_2O_{6-d}$ (L = Pr, Nd, Sm, Eu, Gd, Tb) manganites. *Phys Rev B.* 2002;66:184424.
26. Rakho L Er, Michel C, Lacorre Ph, Raveau B. $YBaCuFeO_{5+\delta}$: A novel oxygendeficient perovskite with a layer structure. *J Solid State Chem.* 1988;73:531.
27. Nakajima T, Kageyama H, Yoshizawa H, Ohoyama K, Ueda Y. Ground state properties of the A-siteordered manganites, $RBaMn_2O_6$ (R = La, Pr and Nd). *J Phys Soc Jpn.* 2003;72:3237.
28. Aliaga H, Magnoux D, Moreo A,Poilblanc D, Yunoki S, Dagotto E. Theoretical study of half-doped models formanganites: Fragility of CE phase with disorder, two types of colossalmagnetoresistance, and charge-ordered states for electron-doped materials. *Phys Rev B.* 2003;68:104405.
29. Trukhanov SV. Peculiarities of the magnetic state in the system $La_{0.70}Sr_{0.30}MnO_{3-\gamma}$ ($0 \leq \gamma \leq 0.25$). *JETP.* 2005;100:95.
30.Trukhanov SV. Magnetic and magnetotransport properties of $La_{1-x}Ba_xMnO_{3-x/2}$ perovskite manganites. *J Mat Chem.*2003;13:347.
31. Rietveld HM. A profile refinement method for nuclear and magnetic structures. *J Appl Crystallogr.* 1969;14:65.
32. Rodriguez-Carvajal J. Recent advances in magnetic structure determination by neutronpowder diffraction. *Physica B.* 1993;192:55.
33. Maignan A, Martin C, Hervieu M, Raveau B, Hejtmanek J. Anomalous magnetotransport properties of the highly A-site mismatched manganite $Nd_{0.7}Ba_{0.3}MnO_3$. *Solid State Commun.*1998;107:363.

34. Roy B, Das S. Magnetic cluster glass behavior and grain boundary effect in$Nd_{0.7}Ba_{0.3}MnO_3$ nanoparticles. *J Appl Phys.* 2008;104:103915.
35. Heilman AK, Xue YY, Lorenz B, Campbell BJ, Cmaidalka J, Meng RL, et al. Distinct insulating state below the Curie point in $Pr_{0.7}Ba_{0.3}MnO_3$. *Phys Rev B.* 2002;65:214423.
36. Jirak Z, Damay F, Hervieu M, Martin C, Raveau B, André G, et al. Magnetism and charge ordering in $Pr_{0.5}Ca_xSr_{0.5-x}MnO_3$ (x=0.09 and 0.5). *Phys Rev B.* 2000;61:1181.
37. Trukhanov SV, Troyanchuk IO, Fita IM, Szymczak H, Bärner K. Comparative study of the magnetic andelectrical properties of $Pr_{1-x}Ba_xMnO_{3-d}$ manganites depending on the preparationconditions. *J Magn Magn Mater.* 2001;237:276.
38. Troyanchuk IO, Khalyavin DD, Trukhanov SV, Szymczak H. Magnetic phase diagrams of the manganites $Ln_{1-x}Ba_xMnO_3$ (Ln = Nd, Sm). *J Phys Cond Matter*. 1999;11:8717.
39. Trukhanov SV, Troyanchuk IO, Trukhanov AV, Fita IM, Vasil'ev AN, Maignan A, et al. Magnetic properties of $La_{0.70}Sr_{0.30}MnO_{2.85}$ anion-deficient manganite under hydrostatic pressure. *JETP Lett.* 2006;83:33.
40. Trukhanov SV, Troyanchuk IO, Pushkarev NV,Szymczak H. Oxygen deficiency effect onmagnetic and electric properties of $La_{0.70}Ba_{0.30}MnO_{3-\gamma}$ ($0 \le \gamma \le 0.30$) manganite withperovskite structure. *JETP*. 2002;95:308.
41. Trukhanov SV, Lobanovski LS, Bushinskii MV, Troyanchuk IO, Szymczak H. Magnetic phase transitions inthe anion-deficient $La_{1-x}Ba_xMnO_{3-x/2}$ ($0 \le x \le 0.50$) manganites. *J Phys Condens Matter*. 2003;15:1783.
42. Quezel-Ambrunaz S. Magnetic structure of the perovskite-like compound $TbMnO_3$. *Bull Soc Mineral Crystallogr*. 1968;91:339.
43. Trukhanov SV, Trukhanov AV,Vasil'ev AN, Maignan A, Szymczak H. Critical behavior of $La_{0.825}Sr_{0.175}MnO_{2.912}$ anion-deficient manganite in the magnetic phase transition region. *JETP Lett.*2007;85:507.
44. Turchenko VA, Trukhanov AV, Bobrikov IA, Trukhanov SV, Balagurov AM. Study of the crystalline and magnetic structures of $BaFe_{11.4}Al_{0.6}O_{19}$ in a wide temperature range. *J Surf Investig.* 2015;9:17.
45. Trukhanov AV, Kostishyn VG, Panina LV, Jabarov SH, Korovushkin VV, Trukhanov SV, et al. Magnetic properties and Mössbauer study of gallium doped M-type barium hexaferrites. *Ceram Int.* 2017;43:12822.
46. Trukhanov SV, Trukhanov AV, Kostishyn VG, Panina LV, Trukhanov AnV, Turchenko VA, et al. Effect of gallium doping on electromagnetic properties of barium hexaferrite. *J Phys Chem Sol.* 2017;111:142.

Figures

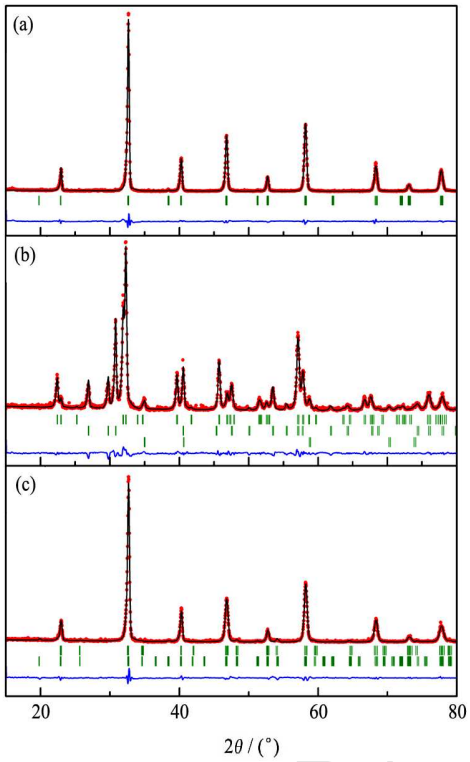

Fig. 1. Observed (solid circles), calculated (solid line), and difference (solid line at the bottom) XRD patterns for Ba-disordered solid solution $Nd_{0.70}Ba_{0.30}MnO_3$ (a), anion-deficient Ba-ordered nanocomposite (1/4)($1.20NdBaMn_2O_5 + 0.80Nd_2O_3 + 1.60MnO$) (b) and oxidized Ba-ordered nanocomposite (1/4)($NdBaMn_2O_6 + 2Nd_{0.90}Ba_{0.10}MnO_{3+\delta}$) at room temperature (c). Bragg reflections are indicated by ticks.

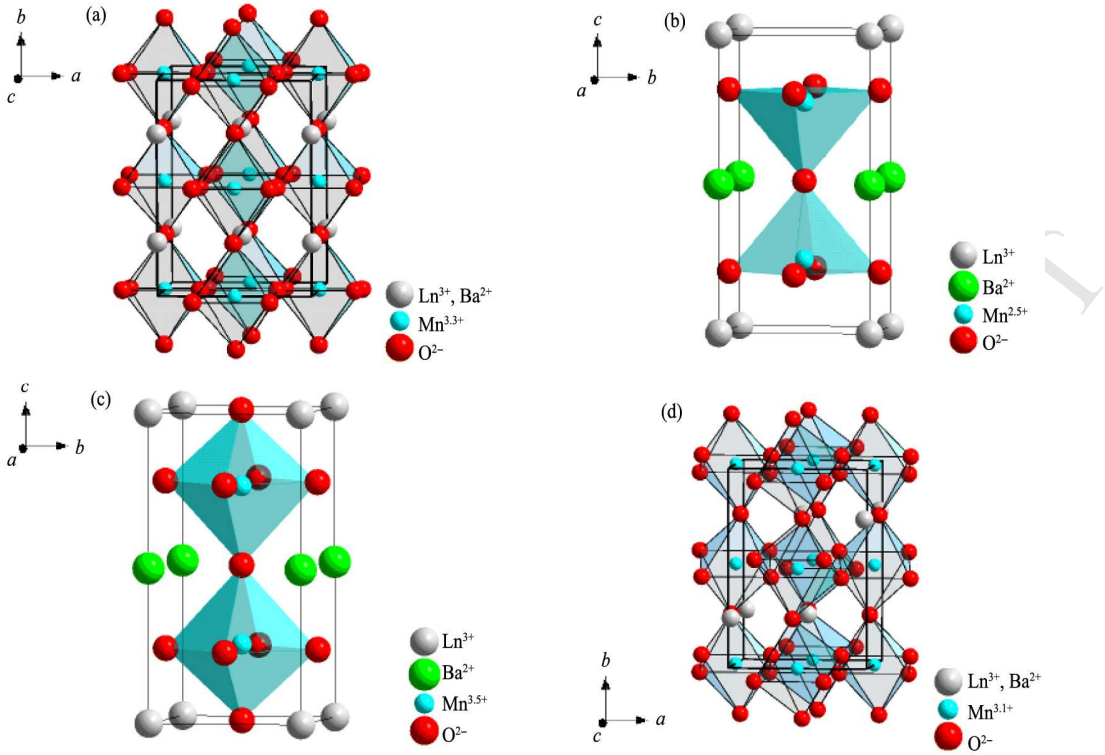

Fig. 2. Schematic representations of the crystal structure for perovskite-like phases: (a) Ba-disordered $Ln_{0.70}Ba_{0.30}MnO_3$; (b) anion-deficient Ba-ordered phase $LnBaMn_2O_5$; (c) stoichiometric Ba-ordered phase $LnBaMn_2O_6$; (d) superstoichiometric Ba-disordered phase $Ln_{0.90}Ba_{0.10}MnO_{3+\delta}$.

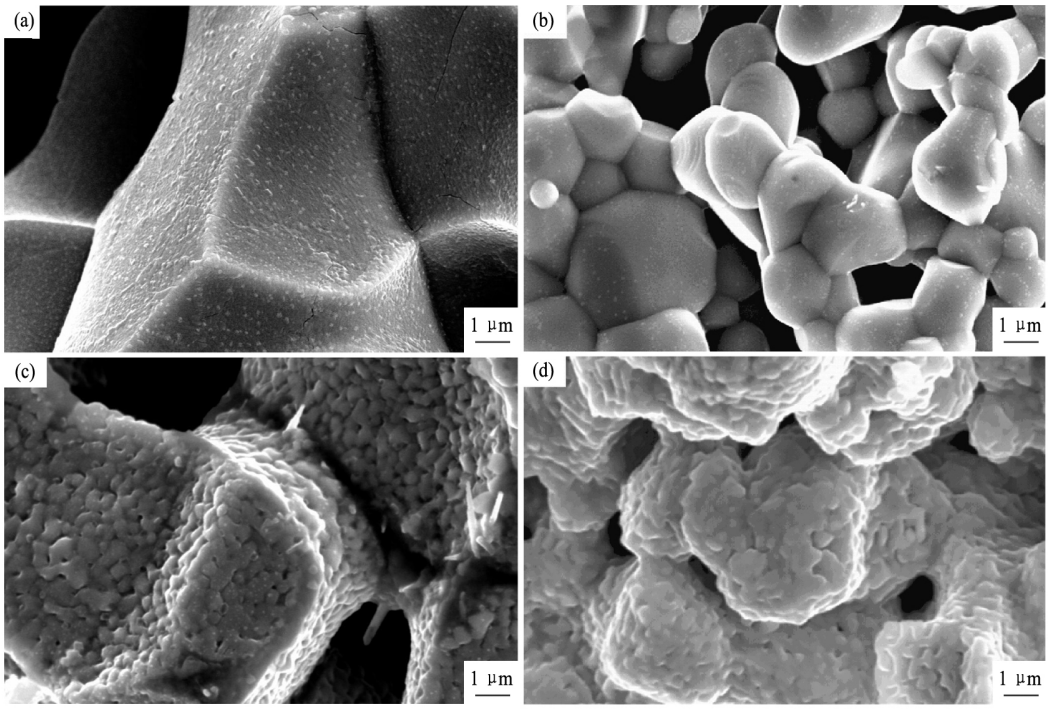

Fig. 3. Surface topography obtained with a scanning electron microscope for parent Ba-disordered solid solution $Pr_{0.70}Ba_{0.30}MnO_3$ (a), parent Ba-disordered solid solution

$Nd_{0.70}Ba_{0.30}MnO_3$ (b), oxidized Ba-ordered nanocomposite (1/4)($PrBaMn_2O_6$ + $2Pr_{0.90}Ba_{0.10}MnO_{3+\delta}$) (c) and oxidized Ba-ordered nanocomposite (1/4)($NdBaMn_2O_6$ + $2Nd_{0.90}Ba_{0.10}MnO_{3+\delta}$) (d)

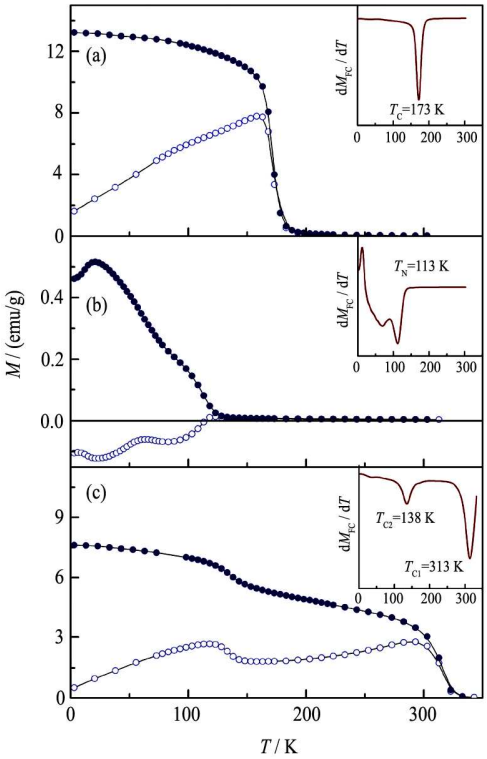

Fig. 4. Temperature dependences of the ZFC (open circles) and FC (closed circles) magnetization in a field of 100 Oe for parent Ba-disordered solid solution $Pr_{0.70}Ba_{0.30}MnO_3$ (a), anion-deficient Ba-ordered nanocomposite (1/4)($1.20PrBaMn_2O_5$ + $(1.60/6)Pr_6O_{11}$ + 1.60MnO) (b) and oxidized Ba-ordered nanocomposite (1/4)($PrBaMn_2O_6$ + $2Pr_{0.90}Ba_{0.10}MnO_{3+\delta}$) (c). The insets show the temperature dependences of the derivative of the FC magnetization for the corresponding samples.

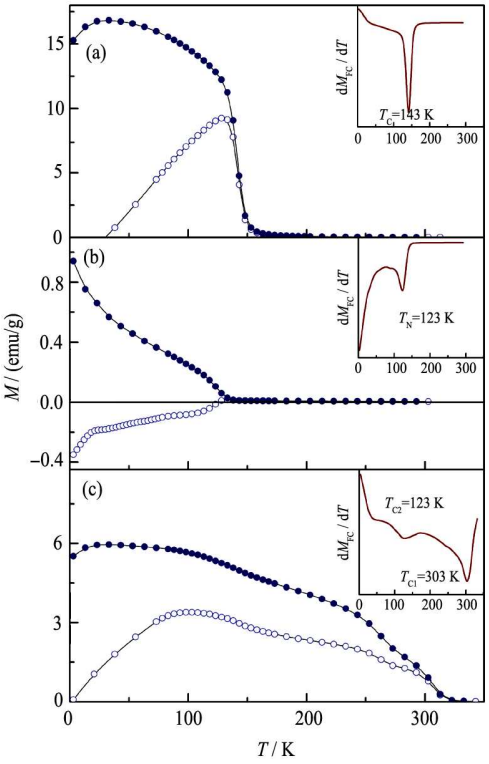

Fig. 5. Temperature dependences of the ZFC (open circles) and FC (closed circles) magnetization in a field of 100 Oe for parent Ba-disordered solid solution $Nd_{0.70}Ba_{0.30}MnO_3$ (a), anion-deficient Ba-ordered nanocomposite $(1/4)(1.20NdBaMn_2O_5 + 0.80Nd_2O_3 + 1.60MnO)$ (b), and oxidized Ba-ordered nanocomposite $(1/4)(NdBaMn_2O_6 + 2Nd_{0.90}Ba_{0.10}MnO_{3+\delta})$ (c). The insets show the temperature dependences of the derivative of the FC magnetization for the corresponding samples.

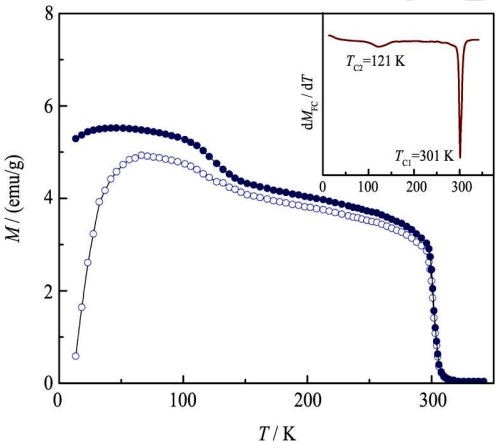

Fig. 6. Temperature dependences of the ZFC (open circles) and FC (closed circles) magnetization in a field of 100 Oe for additionally oxidized Ba-ordered nanocomposite $(1/4)(NdBaMn_2O_6 + 2Nd_{0.90}Ba_{0.10}MnO_{3+\delta})$. The inset shows the temperature dependences of the derivative of the FC magnetization.

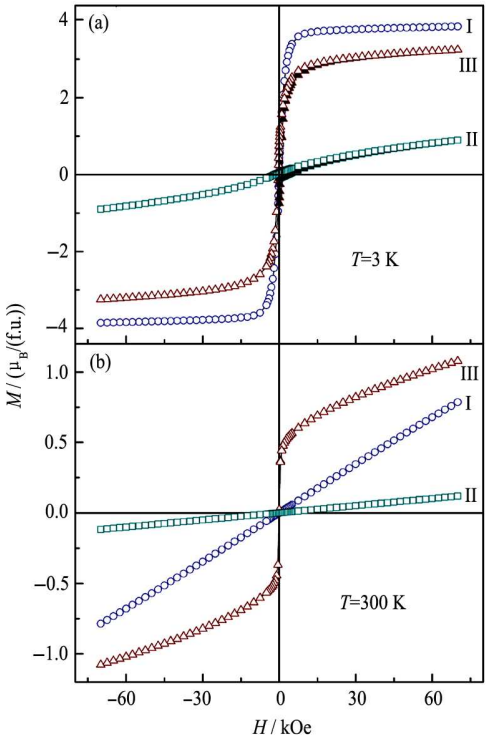

Fig. 7. Field dependences of the magnetization measured at T= 3 K (a) and T= 300 K (b) for parent Ba-disordered solid solution $Pr_{0.70}Ba_{0.30}MnO_3$ (I), anion-deficient Ba-ordered nanocomposite (1/4)(1.20$PrBaMn_2O_5$ + (1.60/6)Pr_6O_{11} + 1.60MnO) (II), and oxidized Ba-ordered nanocomposite (1/4)($PrBaMn_2O_6$ + 2$Pr_{0.90}Ba_{0.10}MnO_{3+\delta}$) (III).

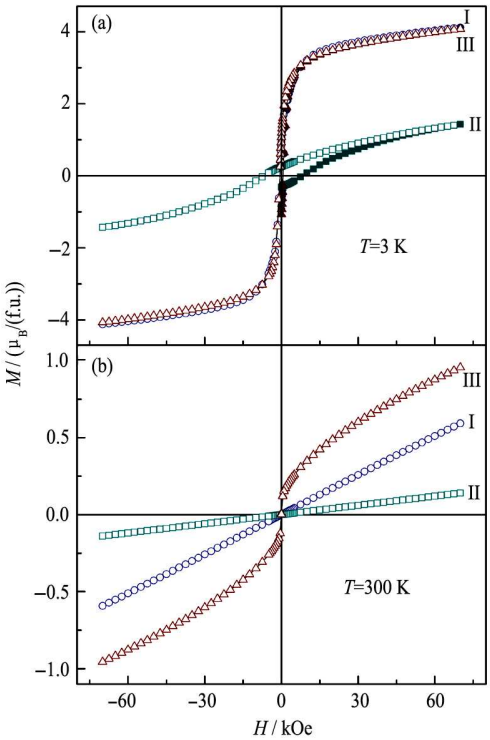

Fig. 8. Field dependences of the magnetization measured at T= 3 K (a) and T= 300 K (b) for parent Ba-disordered solid solution $Nd_{0.70}Ba_{0.30}MnO_3$ (I), anion-deficient Ba-ordered

nanocomposite (1/4)(1.20$NdBaMn_2O_5$ + 0.80Nd_2O_3 + 1.60MnO) (II), and oxidized Ba-ordered nanocomposite (1/4)($NdBaMn_2O_6$ + 2$Nd_{0.90}Ba_{0.10}MnO_{3+\delta}$) (III).

Table 1 Structural parameters for Pr- containing perovskite- like phases at room temperature.

	$Pr_{0.70}Ba_{0.30}MnO_3$	$PrBaMn_2O_5$	$PrBaMn_2O_6$	$Pr_{0.90}Ba_{0.10}MnO_{3+\delta}$
Space group	*Imma*	*P*4/*mmm*	*P*4/*mmm*	*Pnma*
a/nm	0.55252(7)	0.39854(5)	0.8921(6)	0.55142(6)
b/nm	0.77672(8)	0.39854(5)	0.38921(6)	0.77806(7)
c/nm	0.55076(7)	0.77606(9)	0.77625(9)	0.55147(5)
V/nm^3	0.23636	0.12327 {0.24653}	0.11759 {0.23518}	0.23660
$\alpha = \beta = \gamma$(°)	90	90	90	90
Pr, (*x*,*y*,*z*)	(0,¼,–0.004(2))	(0,0,0)	(0,0,0)	(0.021(5),¼,0.999(6))
Ba, (*x*,*y*,*z*)	(0,¼,–0.004(2))	(0,0,½)	(0,0,½)	(0.021(5),¼,0.999(6))
Mn, (*x*,*y*,*z*)	(0,0,½)	(½,½,0.239(4))	(½,½,0.249(5))	(0,0,½)
O1, (*x*,*y*,*z*)	(0,¼,0.435(8))	(½,½,½)	(½,½,½)	(0.469(7),¼,0.012(6))
O2, (*x*,*y*,*z*)	(¾,–0.016(5),¼)	(½,0,0.198(6))	(½,0,0.233(7))	(0.219(7),0.558(6),0.254(7))
O3, (*x*,*y*,*z*)	–	–	(½,½,0)	–
⟨ Mn–O1 ⟩ (nm)	0.1976	0.2048	0.1927	0.1956
⟨ Mn–O2 ⟩ (nm)	0.1951	0.2011	0.1945	0.1863+0.2125
⟨ Mn–O3 ⟩ (nm)	–	–	0.1896	–
⟨ Mn–O1–Mn ⟩ (°)	158.43	180.00	180.00	169.85
⟨ Mn–O2–Mn ⟩ (°)	175.76	161.93	175.18	155.32
⟨ Mn–O3–Mn ⟩ (°)	–	–	180.00	–
R_p (%)	9.21	10.15	10.42	10.42
R_{wp} (%)	13.31	14.21	14.17	14.17
R_B (%)	5.32	3.73	6.33	6.96
χ^2 (%)	2.77	2.98	2.91	2.91

Table 2 Structural parameters for Nd- containing perovskite- like phases at room temperature.

	$Nd_{0.70}Ba_{0.30}MnO_3$	$NdBaMn_2O_5$	$NdBaMn_2O_6$	$Nd_{0.90}Ba_{0.10}MnO_{3+\delta}$
Space group	*Imma*	*P*4/*mmm*	*P*4/*mmm*	*Pnma*
a (nm)	0.55100(8)	0.39626(5)	0.38893(8)	0.54899(8)
b (nm)	0.77523(9)	0.39626(5)	0.38893(8)	0.77755(9)
c (nm)	0.54856(7)	0.77405(9)	0.77310(9)	0.54896(9)
V (nm^3)	0.23432	0.12154 {0.24309}	0.11694 {0.23389}	0.23433
$\alpha = \beta = \gamma$(°)	90	90	90	90
Nd, (*x*,*y*,*z*)	(0,¼,–0.002(3))	(0,0,0)	(0,0,0)	(0.019(3),¼,0.997(3))
Ba, (*x*,*y*,*z*)	(0,¼,–0.002(3))	(0,0,½)	(0,0,½)	(0.019(3),¼,0.997(3))
Mn, (*x*,*y*,*z*)	(0,0,½)	(½,½,0.236(2))	(½,½,0.245(7))	(0,0,½)
O1, (*x*,*y*,*z*)	(0,¼,0.432(9))	(½,½,½)	(½,½,½)	(0.466(9),¼,0.008(8))
O2, (*x*,*y*,*z*)	(¾,–0.012(6),¼)	(½,0,0.195(2))	(½,0,0.230(9))	(0.216(9),0.555(9),0.250(9))
O3, (*x*,*y*,*z*)	–	–	(½,½,0)	–
⟨ Mn-O1 ⟩ (nm)	0.1973	0.2044	0.1974	0.1953
⟨ Mn-O2 ⟩ (nm)	0.1946	0.2007	0.1948	0.1861+0.2122
⟨ Mn-O3 ⟩ (nm)	–	–	0.1892	–
⟨ Mn-O1-Mn ⟩ (°)	158.32	180.00	180.00	168.75
⟨ Mn-O2-Mn ⟩ (°)	174.46	161.72	173.08	154.06
⟨ Mn-O3-Mn ⟩ (°)		–	180.00	–
R_p (%)	9.01	10.11	10.31	10.31
R_{wp} (%)	13.11	14.11	14.11	14.11
R_B (%)	5.52	3.44	6.13	6.84
χ^2 (%)	2.74	2.89	2.99	2.99

Graphic abstrct

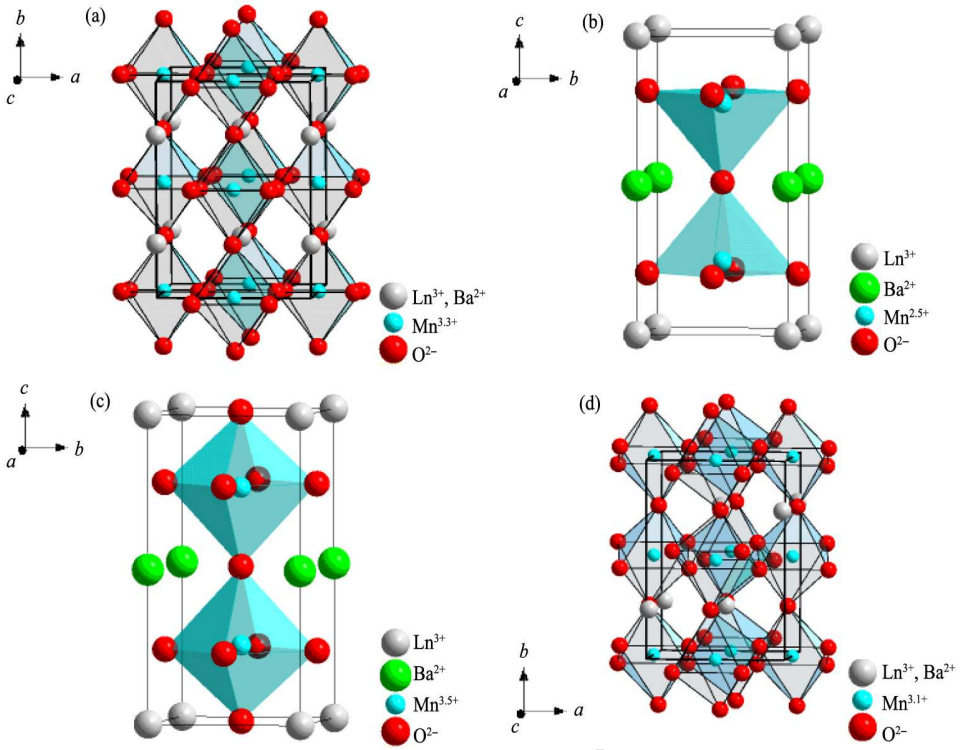

Schematic representations of the crystal structure for perovskite-like phases: (a) Ba-disordered $Ln_{0.70}Ba_{0.30}MnO_3$; (b) anion-deficient Ba-ordered phase $LnBaMn_2O_5$; (c) stoichiometric Ba-ordered phase $LnBaMn_2O_6$; (d) superstoichiometric Ba-disordered phase $Ln_{0.90}Ba_{0.10}MnO_{3+\delta}$